Gravity Wave Activity during Stratospheric Sudden Warmings in the 2007/08 Northern Hemisphere Winter

L. Wang

NorthWest Research Associates Inc., Colorado Research Associates Div., Boulder, Colorado, USA

M. J. Alexander

NorthWest Research Associates Inc., Colorado Research Associates Div., Boulder, Colorado, USA

L. Wang, NorthWest Research Associates Inc., Colorado Research Associates Div., 3380 Mitchell Lane, Boulder, CO 80301, USA (lwang@cora.nwra.com)

Abstract. We use temperature retrievals from the Constellation Observing System for Meteorology, Ionosphere and Climate (COSMIC)/Formosa Satellite Mission 3 (FORMOSAT-3) and Challenging Minisatellite Payload (CHAMP) Global Positioning Satellite (GPS) radio occultation profiles and independent temperature retrievals from the EOS satellite High Resolution Dynamics Limb Sounder (HIRDLS) and Sounding of the Atmosphere using Broadband Emission Radiometry (SABER) aboard the TIMED satellite to investigate stratospheric sudden warming (SSW) events and the accompanying gravity wave (GW) temperature amplitudes in the 2007/08 Northern Hemisphere winter. We identify four SSW events (including a major one) occurring from late January to late February in 2008. We detect enhanced GW amplitudes in the stratosphere and subdued GW amplitudes in the lower mesosphere during the warming events. The timing of GW enhancement/suppression and warming/cooling events was generally close (within a couple days). We also find that stratospheric GW amplitudes were generally larger at the polar vortex edge, and smaller in the vortex core and outside of the vortex, and stratospheric GW amplitudes were generally small over the north Pacific. Using a simplified GW dispersion relation and a GW ray-tracing experiment, we demonstrate that the enhanced GW amplitudes in the stratosphere during SSWs could be explained largely by GW propagation considerations. The existence of GW critical levels (the level at which the background wind is the same as the GW phase speed) near the stratopause during SSWs would

block propagation of GWs into the mesosphere and thus could lead to the observed subdued GW activity in the lower mesosphere.

Since this is the first study to analyze the COSMIC and CHAMP GPS temperature retrievals up to 60 km in altitude, we compare the GPS analysis with those from HIRDLS and SABER measurements. We find that the temporal variability of zonal mean temperatures derived from the GPS data is reasonable up to $\sim$ 60 km in altitude, but the GPS data were less sensitive to SSWs than HIRDLS and SABER. GW analysis from GPS is consistent with HIRDLS up to $\sim$ 35 km in altitude but it seems that the small-scale variability at higher altitudes revealed in the GPS data is questionable.

1. Introduction

Stratospheric sudden warmings (SSWs) are large-scale transient events in the winter polar middle atmosphere. They affect the middle atmosphere structure and general circulation profoundly [*Andrews et al.*, 1987] and could also have significant impacts on weather in the troposphere [*Baldwin and Dunkerton*, 2001]. During an SSW event, the zonal mean temperatures in the polar middle stratosphere increase by several tens of Kelvins within a few days. The warming is accompanied by the weakening of the polar vortex and westerly winds (and even complete breakdown of the polar vortex and reversal of zonal mean zonal winds in the case of a major event). SSWs are also observed to be accompanied by significant coolings in the mesosphere.

SSWs are the most dramatic example of dynamical coupling of the lower and middle atmosphere. They are commonly believed to be caused by the interaction of wavenumber 1 or 2 Rossby waves originating from the lower atmosphere with the mean flow [*Matsuno*, 1971]. When those westward propagating waves enter the polar stratosphere, they exert a westward acceleration (thus weakening or even reversing the normally westerly flow) through wave dissipation or wave transience (i.e., the Eliassen-Palm flux divergence). This westward zonal force is partly offset by the Coriolis force and induces a poleward residual circulation causing sinking motion below and poleward of the forcing region. The adiabatic temperature changes give rise to the warming observed in the polar stratosphere. Due to mass balance, the poleward residual circulation also causes adiabatic ascent above and poleward the forcing region, thus explaining the accompanying mesospheric cooling [*Matsuno and Nakamura*, 1979].

Due to the dramatic change of the background atmosphere within a very short period of time, SSWs affect gravity wave (GW) propagation and transmission in the middle atmosphere profoundly. For example, orographically generated stationary GWs would be absorbed by the mean atmosphere as they approached the zero mean zonal wind level in the course of a SSW. Such interaction of GWs and winds during SSWs would have significant impacts on the structure and general circulation in the mesosphere as the resulting reduction in GW drag and diffusion would imply a reduced amplitude for mean meridional circulation which is induced by GW breaking. The reduced meridional circulation during SSWs implies a colder winter polar mesosphere which is normally much warmer than radiative equilibrium. As argued by *Holton* [1983], this mechanism explains better the observed broad depth of mesospheric coolings than the secondary meridional circulation mechanism proposed by *Matsuno and Nakamura* [1979] mentioned above. The modified GW properties during SSWs could also affect the mean atmosphere below the middle stratosphere via the downward control principal [*Haynes et al.*, 1991; *Garcia and Boville*, 1994].

There have been a few observational studies to examine GW activity during SSWs in the past few decades. *Duck et al.* [1998] examined the relationship between GWs and SSWs using lidar temperature measurements in the stratosphere over Eureka (80°N, 86°W). They detected increased GW activity in the polar vortex jet during the warming. *Ratnam et al.* [2004] examined GW activity during the unprecedented major SSW in the Southern Hemisphere in 2002 using the CHAMP GPS temperature profiles. They found that GW potential energies in the stratosphere below 30 km increased three-fold during the event. *Wang et al.* [2006] analyzed rocket soundings obtained from the MaCWAVE winter campaign and found clear evidence of topographic GWs approaching their critical levels during an SSW event. *Dowdy et al.* [2007] investigated the dynamical response of the polar mesosphere and lower thermosphere to SSWs using MF radar horizontal wind data at two Antarctic and two Arctic sites. They found that SSWs had a variable effect on mesospheric GW activity, depending on factors such as location, GW frequency, and the individual SSW event. At one station (Davis, 69°S, 78°E), GW variance was reduced by $\sim$ 50%, while at Syowa (69°S, 40°E) there was an increase of $\sim$ 20% in variance.

All the studies cited above analyzed either data from a single or limited locations or a global dataset but with a very sparse spatial coverage (note that the CHAMP data has only $\sim$ one hundred or so occultations per day). In addition, those CHAMP GPS studies analyzed the global data only below $\sim$ 35 km. In comparison, the COSMIC data processed by the University Corporation for Atmospheric Research (UCAR)'s COSMIC Data Analysis and Archive Center (CDAAC) has a ten-fold increase of daily occultations [*Rocken et al.*, 2000] and the temperature retrievals reach an altitude as high as 60 km. The UCAR CDAAC has also reprocessed the CHAMP GPS data with an altitude range from near the ground up to 60 km. In this study, we use both the UCAR CDAAC COSMIC and CHAMP GPS temperature retrievals between 20 and 60 km to examine SSWs occurring during the 2007/08 Northern Hemisphere winter and to analyze the corresponding GW characteristics so that we can gain some understanding of the interactions between SSWs and GWs for this particular season. Since this is the first study to utilize the COSMIC and CHAMP GPS temperature data above 35 km in altitude, independent temperature retrievals from HIRDLS and SABER are used to supplement and validate the GPS analysis at upper levels.

The paper is organized as follows. Section 2 describes the datasets used in this study. Sections 3 and 4 show the temporal variability of zonal mean temperatures and zonal mean GW temperature amplitudes at high latitudes. Section 5 discusses the geographic variability of GW amplitudes. A GW ray-tracing experiment is presented in Section 6 to interpret the observed temporal variability of GW amplitudes in the stratosphere. In the end, the summary and conclusions are given.

2. Data

The concept of atmospheric profiling by GPS radio occultation (RO) was first introduced by *Yunck et al.* [1988]. GPS RO is a space-borne remote sensing technique providing accurate, all-weather, high vertical resolution profiles of atmospheric variables. Satellites in low-Earth orbit (LEO), as they rise and set relative to the GPS satellites, measure the frequency change of the GPS dual-frequency signals. The Doppler-shifted frequency measurements are used to compute the bending angles of the radio waves, which are reduced to derive the atmospheric refractivity. In the neutral atmosphere, the refractivity is further reduced to temperature, pressure and water vapor profiles. GPS/MET was the first demonstration of the GPS RO technique [*Ware et al.*, 1996]. There were a few follow-on GPS experiments. They include the German Challenging Minisatellite Payload (CHAMP) and the Argentine Satellite de Aplicaciones Cientificas-C (SAC-C) missions both of which were launched in 2000. Most recently, the Constellation Observing System for Meteorology Ionosphere and Climate (COSMIC)/Formosa Satellite 3 (FORMOSAT-3) [*Rocken et al.*, 2000] was successfully launched into orbit in April 2006. Compared with previous GPS missions, COSMIC provides an unprecedentedly large number of radio occultations. Since the pioneering work of *Tsuda et al.* [2000], various authors have used those different GPS datasets to study stratospheric GWs [e.g., *de la Torre et al.*, 2004; *Ratnam et al.*, 2004; *Baumgaertner and McDonald*, 2007; *Hei et al.*, 2008; and *Alexander et al.*, 2008].

In this study, we analyze the Version 2.0 COSMIC and CHAMP dry temperature profiles processed by the UCAR CDAAC. We focus on the period from 1 December 2007 to 31 March 2008 when there were $\sim$ 1500 and 150 daily soundings from COSMIC and CHAMP, respectively. Both COSMIC and CHAMP temperature data have a vertical resolution of $\sim$ 1 km and their accuracy is sub-Kelvin. Since COSMIC and CHAMP data have similar data quality, we merge them to gain better spatial coverage. The locations of the merged GPS daily RO occultations are roughly evenly distributed in space and local time and their daily maximum latitude routinely reaches within 2° of the poles so the GPS data are particularly useful for studying polar phenomena such as SSWs. Another advantage of the GPS data (e.g., CHAMP and potentially COSMIC) is that they can have longer temporal coverage than many other satellite data. The GPS RO retrievals are available from near the ground up to 60 km but we analyze temperatures only above 20 km to emphasize the stratosphere and lower mesosphere region.

To supplement and validate the GPS analysis especially at upper levels, we also use independent temperature retrievals from the EOS/HIRDLS [*Gille et al.*, 2008] (Version 4) and TIMED/SABER [*Mlynczak and Russell*, 1995] (Version L2A) when and where they overlap with the GPS data. All three datasets have global coverage, though SABER can sample only one hemisphere's high latitude region at a time due to the TIMED satellite's yaw cycle and the highest latitude that HIRDLS reaches is $\sim$ 80°N. Also, relevant to the time period that we are studying, we miss quite a few days of data for HIRDLS. Unlike

GPS, both HIRDLS and SABER sample along single measurement tracks per orbit. Both GPS and HIRDLS have a relatively high vertical resolution ($\sim$ 1 km) so in theory they can be used to study GWs of vertical wavelengths as short as 2 km. For HIRDLS, the instrument field of view is 1.2 km, so the shortest wave may be closer to 2.4 km. Note that in practice, it would be difficult to revolve waves with scales very close to the Nyquist vertical wavelength mentioned above. *Alexander el al.* [2008] have used the HIRDLS data to derive global estimates of GW momentum flux. SABER has a relatively coarser vertical resolution of $\sim$ 2 km.

3. Temporal Variability of Zonal Mean Temperatures

Figure 1 shows the time-altitude contour of zonal average of daily mean GPS temperatures at 70°N (with a latitudinal bin of 10°) and time-latitude contour of zonal average of daily mean GPS temperatures at 10 hPa pressure level between 1 December 2007 and 31 March 2008. The time-latitude contour of zonal mean zonal wind analysis data from the European Centre for Medium-Range Weather Forecasts (ECMWF) (ds111.2) [*Trenberth*, 1993] is also shown in Figure 1.

The polar stratosphere was generally relatively quiet until late January when the stratospheric temperatures warmed up quickly and several episodes of SSWs occurred. For example, at 30 km in altitude, the zonal mean temperatures increased by more than 30 K within only a couple days before 25 January 2008. More episodes of dramatic stratospheric temperature increase followed. We can clearly identify four SSW events. All of them showed the classic downward progression of the warm stratospheric temperatures, the accompanying mesospheric coolings (with little time difference between stratospheric warmings and mesospheric coolings in those cases), the lowered stratopause height, the reversed meridional temperature gradient, and the weakening (or even reversal) of the zonal wind. If we define the date of each event by the time when the meridional temperature gradient was positive and its value was maximum, the four SSWs occurred at 25 January, 2 February, 16 February, and 23 February of 2008, respectively. Among the events, the 23 February one is a major event which is characterized by the reversal of the zonal wind at 10 hPa. The 25 January event is extraordinary in that its temporal change of temperatures is the largest among the four even though it is a minor one by the WMO definition. From the ECMWF analysis geopotential height data (not shown), these SSWs are mostly of the zonal wave-1 type, though also with some wave-2 component.

Note that there could be large uncertainties in GPS temperature retrievals at upper levels (above $\sim$ 35 km) due to noise and the residual ionospheric effects [*Kuo et al.*, 2004]. As noted by *Kuo et al.* [2004] though, the residual ionospheric effects in the GPS RO retrievals are the smallest during solar minimum at night time. Indeed, the time period considered in this study happens to correspond to a solar minimum. Also, we have conducted a separate zonal mean analysis of the night-time GPS data only and found that the results are largely the same as those reported here.

The temperature retrievals at upper levels are also affected by *a priori* information used for the optimal estimation of bending angles and integration of the hydrostatic equation in the CDAAC GPS RO inversions. Specifically, the CDAAC uses the NCAR climatology described in Section 4 of [*Randel et al., 2002*] for the optimal estimation of bending angles and initialization of temperatures at 80 km to calculate the hydrostatic integral (Note that other GPS RO processing centers may use different climate models for those purposes.) The detailed descriptions of the optimal estimation of bending angles and the hydrostatic integral applied at the CDAAC are given by *Kuo et al.* [2004] and *Lohmann [2005]*. As a result of using *a priori* in the inversions, the temperature retrievals are a mixture of real neutral atmospheric signals, *a priori* information, and noise and the residual ionospheric effects (as discussed above), and the relative contribution from *a priori* increases significantly with altitude. Hence, the temperature retrievals at upper levels can be severely diluted by *a priori* information. Since the temporal variability of temperatures at upper levels exhibits a time scale of from several days up to $\sim$ a week during SSWs (Figure 1a) whereas the time scale of *a priori* used by the CDAAC is on the order of a month, the temporal variability of zonal mean temperatures at upper levels is likely due to true geophysical signals.

It would be interesting to compare the GPS results with those from HIRDLS and SABER (Figure 2). Since HIRDLS data are reported at pressure levels while SABER data are reported at geometric altitudes, the comparison is made at pressure and altitude levels for them, respectively (the GPS products include both altitude and pressure information). For the comparison with HIRDLS, we interpolate the GPS data to the HIRDLS pressure levels (which have an equivalent pressure altitude resolution of $\sim$ 0.672 km if a pressure scale height of 7 km is assumed) before calculating their differences shown in Figure 2b. For the comparison with SABER, we interpolate both the SABER and GPS data linearly to a regular vertical resolution of 1 km before calculating their differences shown in Figure 2d. Note that there datasets used in the daily and zonal mean analysis shown in Figure 2 have different spatial and local-time sampling. It is evident that all three datasets are capable of capturing the SSW events in the stratosphere and to first order the temporal variability of the GPS data at upper levels is generally similar to those from the other two datasets. Note that HIRDLS global mean temperatures are known to have a cold bias at upper levels [*Gille et al.*, 2008]. This could possibly explain the overall warmer GPS temperatures than HIRDLS at upper levels. It is interesting to note that the GPS RO zonal mean temperatures are somewhat less sensitive to warmings than HIRDLS and SABER and this could be due to the optimization applied in the GPS RO inversions, that dilutes the neutral atmosphere signals with *a priori* as discussed above. Nevertheless, the comparison among the datasets suggests that the temporal variability of GPS zonal mean temperatures at upper levels is realistic.

Finally, to assess the contribution of the real neutral atmospheric signals to the GPS temperature retrievals used in this study, we analyze the “zmwv” parameter in the CDAAC products. “zmwv” is the median height of the weighting vector for the observational bending angle and at this height there is 50% of *a priori* in the optimized bending angle (Sergey Sokolovskiy, personal communication). This parameter varies with each individual RO occultation and for the occultations used in the analysis in Figure 1a, it varies mostly between 40 and 50 km with a mean value of $\sim$ 44 km. We have also noticed that the value of “zmwv” is generally larger at high latitudes in winter (not shown). This factor together with the better spatial coverage of the GPS RO data in the polar regions than other satellite data (as described in Section 2) makes the GPS RO data valuable for studying the polar middle atmosphere.

4. Temporal Variability of Gravity Wave Amplitude

As mentioned in Section 2, both GPS and HIRDLS have a rather good vertical resolution, so they can be used to study small-scale phenomena such as GWs. GW analysis depends on the extraction of GW perturbations, i.e., the removal of the “background”.

Previous studies estimated GW temperature perturbations by applying a vertical wavelength (λ_z) filter directly to individual GPS temperature profiles [*Tsuda et al.*, 2000; *Ratnam et al.*, 2004; *de la Torre et al.*, 2004; *Baumgaertner and McDonald*, 2007]. In fact, large-scale waves such as Kelvin waves can have similar λ_z as GWs. For example, *Holton et al.* [2001] identified from radiosonde data Kelvin waves of zonal wavenumber 2 and 4 with vertical wavelength of $\sim$ 4.5 km and 3-4.5 km, respectively. Therefore, filtering temperature profiles with respect to λ_z alone does not clearly separate global-scale waves and GW signals. The combined COSMIC and CHAMP data provide nearly ten times more daily profiles than previous GPS missions, thus giving us the opportunity to define the background temperature on the basis of horizontal scale and to separate the GWs from the global-scale waves on this basis.

We obtain GW perturbations using the following procedure (which is analogous to *Alexander et al., 2008*). First, each profile is interpolated in altitude to a regular 200-m resolution (which is oversampling for both GPS and HIRDLS). Next, each day's profiles are gridded to $15° \times 10°$ longitude and latitude resolution. The S-transform is performed as a function of longitude for each latitude and each altitude, giving zonal wavenumber 0-12 as a function of longitude. Note that the S-transform is a continuous wavelet-like analysis [*Stockwell et al.*, 1996] that uses an absolute phase reference, and the longitudinal integral of the transform recovers the Fourier transform. In this study we reconstruct zonal wavenumbers 0-6 to define the "large-scale" temperature variation. This large scale, interpolated back to the positions of the original profiles, is subtracted leaving perturbations with horizontal fluctuations shorter than wavenumber 6. We have tested the sensitivity of the analysis results using different cut-off zonal wavenumbers ranging from 3 to 10 (whenever the data spatial coverage allows this) and have found that the major results reported here remain largely the same. Note that the above procedure to derive GW background profiles neglects any time variations of large-scale waves within one day. Finally, we derive GW temperature amplitudes as a function of altitude from the temperature perturbations using the S-transform.

Figure 3 shows the time (daily)-altitude contours of zonal averaged GW temperature amplitudes at high latitudes. Evidently, there were enhancements of GW activity in the stratosphere during SSWs. At 70°N, for example, GW temperature amplitude increased by a factor of 3 on 25 January 2008 in comparison to the time when the atmosphere was less disturbed during December 2007 and early January 2008. GW amplitudes were also smaller after the late February major warming event when the polar middle atmosphere started to transition from the winter to summer state. In the 25 January event, for instance, there was also a downward progression of GW signals associated with the warming event (Figure 3d).

As mentioned in the Introduction, the enhancement of GW activity during SSWs has been reported in previous studies [e.g., *Duck et al.*, 1998; *Ratnam et al.*, 2004]. It is interesting though that the timing of GW enhancement was very close with that of the SSWs in the 2007/08 Northern Hemisphere winter (generally within 1 or 2 days) whereas *Ratnam et al.* [2004] reported enhanced GW potential energy appearing 10 days earlier than the major Southern Hemisphere SSW in late winter/spring of 2002.

We showed in Figure 3 GPS GW analysis no higher than 35 km in altitude. Figure 4 compares zonal mean GW temperature amplitudes as a function of time and vertical wavelength from both GPS and HIRDLS temperature retrievals at selected altitudes, some of which are higher than 35 km. The temporal variability of GW amplitudes from HIRDLS is rather consistent with that from GPS at lower altitudes (below $\sim$ 35 km) and confirms the GPS observations that there was enhancement of GW amplitudes in the stratosphere during SSWs. At 40 km and above, however, the two become opposite. The GPS results continue to reveal larger GW amplitude during SSWs at upper levels but the HIRDLS results show that GW amplitudes were subdued at upper levels in the lower mesosphere during SSWs. Note that in Figure 4, 50 km was still in the upper stratosphere except during the SSWs.

Bear in mind that we derive GW perturbations by removing large-scale zonal structures reconstructed from the gravest zonal modes derived from the S-transform analysis, so the GPS and HIRDLS GW analyses would be different if their respective zonal mode estimates were different. Actually the amplitude and phase of the gravest zonal modes among the various datasets are very consistent below $\sim$ 40 km but the GPS results are quite different from those from HIRDLS and SABER at higher altitudes (not shown). To exclude the possibility that such differences in zonal modes caused the differences in GW analysis, we conduct a separate analysis using the conventional band-pass filter method (as by *Tsuda et al.* [2000]) to derive GW perturbations for both GPS and HIRDLS (not shown), but the results are the same.

The existence of GW critical-levels due to the reversal of zonal winds during SSWs act to block most GWs before they can reach the mesosphere, therefore we expect that there should be a reduction of GW signals in the mesosphere during SSWs [*Holton*, 1983]. Also, there has been direct observational evidence supporting this argument. For example, *Wang et al.* [2006] observed exceptionally strong GW signals in the stratosphere but very week GW signals in the mesosphere in the course of an SSW event during the winter MaCWAVE campaign. Thus, we have more confidence in the HIRDLS results at upper levels, and it is likely that the small-scale variability shown in the GPS data above 35 km might be due to the GPS retrieval uncertainty at upper levels. The residual ionospheric effects are normally the largest source for GPS temperature retrieval uncertainties at high altitudes [*Kuo et al.*, 2004]. However, a separate GW analysis using only the night-time GSP data to minimize the residual ionospheric effects still shows the same seemingly erroneous temporal variability at upper levels. Also, if the small-scale variability is noise, it is unclear why noise would increase during SSW events. Therefore further studies are needed to pinpoint the underlying causes of the GPS retrieval uncertainty at upper levels.

5. Geographic Variability of Gravity Wave Amplitude

So far we have examined only the zonal mean temperatures and GW amplitudes. The high horizontal resolution of the combined COSMIC/CHAMP dataset allows us to investigate the geographic variability of GW amplitudes. Figure 5 shows the stereographic projected contoured maps of GW amplitudes averaged between 30 and 35 km from the GPS for the four days when the SSWs occurred. Also shown are the stereographic projected contoured maps of daily mean zonal velocity components, wind speeds, and geopotential heights at the 10 hPa pressure level from the ECMWF analysis. Here we use the wind speed and geopotential height contours to identify the location of the polar vortex. The polar vortex was generally well-defined except on 23 February 2008 when it was completely broken down (which is characteristic of a major SSW).

All four days displayed large zonal asymmetry in GW amplitudes. In addition it appears that there is a fairly good correspondence between GW amplitudes and the strength of polar vortex winds during weak warmings (top three rows): GWs were generally larger near the polar vortex edge and smaller in the vortex core and outside the vortex during SSWs. This observation does not hold for the major SSW when the polar vortex itself was poorly defined (bottom row). Such an association between larger GW amplitudes and the locations of polar vortex edges is also a normal feature during undisturbed conditions (not shown).

Some previous studies also examined the relationship between the polar vortex position and GW activity during SSWs. For example, *Duck et al.* [2001] analyzed GW activity from lidar temperature measurements over Eureka during the 1992/93 - 1997/98 wintertime campaigns and found high GW activity in the vortex jet after late December and low GW activity in the vortex core, outside of the vortex altogether, and in the vortex jet before mid-December. *Ratnam et al.* [2004] reported enhancement of GW energies near the polar vortex edge and outside the polar vortex but weak GW energies inside the vortex during the 2002 Southern Hemisphere major warming event. Except for some differences in details, our results are generally consistent with those previous studies.

The association between larger stratospheric GW amplitudes and stronger winds (which often had a larger eastward component) in the same altitude range during most of the days examined is also observed in the stratospheric Aleutian high pressure system where winds were normally very weak and often had westward wind components. Those observations are likely evidence of selective transmission of GWs by the spatially varying background winds [*Dunkerton and Butchart*, 1984].

6. Mechanism for Stratospheric Gravity Wave Enhancements during SSWs

Figures 3 and 4 showed that GW amplitudes in the stratosphere were generally enhanced during SSWs. Such enhancements could be explained to some extent by the GW propagation considerations. During SSWs, the zonal wind reversal (or weakening) could refract GWs arising from the lower atmosphere in such a way that more waves could be observed by GPS and HIRDLS in the stratosphere (i.e., the so-called observational window effect introduced by *Alexander* [1998]). As the simplest illustration of this mechanism, we estimate the vertical wavelength of a stationary GW at the 10 hPa pressure level using the following formula

$$\lambda_z = 2\pi \frac{\overline{u}}{N} \tag{1}$$

where λ_z is vertical wavelength, $\overline{u}$ is background zonal wind, and N is the background buoyancy frequency. Equation (1) is a good approximation of the full dispersion relation for zonally propagating stationary GWs. Figure 6 displays the daily time series of λ_z calculated from this simplified dispersion relation using zonal mean zonal winds and N at 70°N from the Goddard Earth Observing System Version 5.0.1 (GEOS-5) analysis data [*Rienecker et al.*, 2008]. Note that our analysis can resolve GWs with vertical scales no shorter than twice the vertical resolution of the GPS and HIRDLS data ($\sim$ 1 km). In practice, the limited height range of the profiles means we cannot resolve GWs of ultra-long vertical scales, nor waves with scales very close to the Nyquist vertical wavelength. Given this consideration and the results shown in Figure 4, it is reasonable to choose the 4-10 km vertical wavelength observational window for this particular analysis. Evidently, Figure 6 demonstrates that the rapidly changing zonal winds during SSWs refract GWs significantly and very rapidly to vertical scales that are most visible to the GPS and

HIRDLS observations. The estimated vertical wavelength for the third event is shorter than 4 km but still longer than the Nyquist vertical wavelength.

There is generally large zonal asymmetry in zonal winds in the polar winter middle atmosphere and such zonal asymmetry can lead to the so-called GW selective transmission effects discussed by *Dunkerton and Butchart* [1984]. Hence, we conduct a GW ray-tracing experiment to see how both temporally and longitudinally varying zonal winds during SSWs could affect GWs that fall into the observational window of the GPS and HIRDLS data. In this experiment, we launch rays at an altitude of 10 km along the 70°N latitude band with a longitudinal interval of 5°. We use a constant source spectra with zonal phase speed ranging from -10 to 10 ms^{-1} with a resolution of 0.2 ms^{-1}. We choose such a narrow band of phase speed centered around zero because *Alexander and Rosenlof* [2003] argued that the GW source spectra in extratropics should be quasi-stationary in winter and fall as constrained from satellite observations. The source spectra horizontal wavelength is taken to be 300 km, being close to the statistics of GW parameters reported by *Wang et al.* [2005]. The horizontal resolution of GPS RO temperature retrieval is $\sim$ 150 km along the line-of-sight of the occultation path and $\sim$ an order of magnitude small across the path. Smoothed daily mean GEOS-5 analysis data are used to represent the background atmosphere through which the waves are propagating. We use the Gravity-wave Regional Or Global RAy Tracer (GROGRAT) [*Marks and Eckermann*, 1995] as the GW ray-tracing solver. GROGRAT is capable of performing 4-D GW ray-tracing. For simplicity, only vertical propagation is considered in this experiment.

Figure 7 shows the time series of the normalized probability of observing a GW in the altitude range of 25 to 35 km in the observational window of 4-10 km in vertical wavelength along the latitudinal band of 70°N. The probability is normalized in such a way that the maximum and minimum value of probability in the whole time series is linearly scaled to 1 and 0, respectively. The simulation results suggest that the GW propagation considerations alone could largely explain the enhanced stratospheric GW activity during SSWs. In addition, the propagation considerations can also explain the observed reduced GW amplitudes in the lower mesosphere, as mentioned above.

Another possible cause for GW temporal variability is the temporal variability of GW sources. GWs are spontaneously emitted when unbalanced flows are restored to a more balanced state, and the so-called spontaneous imbalance is one of the major sources of GWs, especially in the extratropics. Figure 8 shows the daily time series of mean GPS GW amplitudes between the altitude range of 20 and 25 km and north of 50°N. It also shows the daily time series of mean magnitudes of ΔNBE at the 350 hPa pressure level between 50°N and 85°N. ΔNBE is the residual of nonlinear balanced equation [*Zhang et al.*, 2001]:

$$\Delta \mathrm{NBE} = 2J(u, v) + f\zeta - \nabla^2\Phi - \beta u \tag{2}$$

where u and v are the zonal and meridional horizontal velocity component, respectively, f is the Coriolis parameter, β is the meridional gradient of the Coriolis parameter, Φ is the geopotential height, ζ is the relative vorticity, and J is the Jacobian term $(J_{xy}(u, v) \equiv (\partial u/\partial x \cdot \partial v/\partial y) - (\partial v/\partial x \cdot \partial u/\partial y)$. The above formula is derived from scale analysis of the divergence equation and it can be shown that ΔNBE should be zero if the flow is perfectly balanced. The magnitude of ΔNBE has been used as an indicator of GW source regions in unbalanced flow [e.g., *Zhang et al.*, 2001]. We evaluate ΔNBE using the GEOS-5 analysis data. The 350 hPa pressure level is where ΔNBE is found to be the largest in the troposphere for this analysis. There is a significant correlation between GW amplitudes and ΔNBE (with a correlation coefficient of 0.42), but the two variables do not exhibit high one to one correspondence as shown in Figure 8. Another likely GW source in the polar winter is topography. We have evaluated the correlation between the strength of low-level winds (as a crude proxy for the strength of topographic wave source) from the GEOS-5 analysis data and stratospheric GW amplitudes and have found that the two variables have an even lower correspondence (not shown). Obviously, GWs can experience profound modulations and changes when they propagate away from their sources, therefore it is difficult to separate source effects and propagation effects in those simple correlational analyses. To understand fully the respective roles of wave sources and propagation in causing the observed GW temporal variability, more detailed modeling studies are needed.

7. Summary and Conclusions

We investigate the stratospheric and lower mesospheric temperatures and GW amplitudes during the 2007/08 Northern Hemisphere winter using the COSMIC and CHAMP GPS temperature retrievals and independent HIRDLS and SABER temperature data.

We identify four SSW events which occurred between late January to late February in 2008 (Figure 1). All the events showed the classic downward progression of warm stratospheric temperatures, the accompanying mesospheric coolings, the lowered stratopause heights, the reversed meridional temperature gradients, and the weakening or reversal (in the case of the major warming event in late February) of the zonal winds. For the SSWs examined in this study, there were little or no time lags between stratospheric warmings and mesospheric coolings.

We notice a large increase of GW amplitudes at high latitudes in the stratosphere during SSWs in the 2007/08 Northern Hemisphere winter and the timing of the GW enhancements with respect to SSWs was generally very close (within a couple days at most) (Figures 3-4). *Ratnam et al.* [2004] also noted enhanced GW energies during an SSW event in the Southern Hemisphere in 2002 but the stratospheric GW energy spike occurred $\sim$ ten days earlier than the warming event. The enhancements of stratospheric GW activity during SSWs can be primarily explained by GW propagation considerations. During SSWs, the zonal wind reversal (or weakening) could refract GWs arising from the lower atmosphere in such a way that more waves could be observed by GPS and HIRDLS in the stratosphere. The simple vertical wavelength estimates (Figure 6) and GW ray tracing results (Figure 7) support this wave refraction interpretation. We also notice a decrease of GW amplitudes in the lower mesosphere during SSWs (above $\sim$ 35 km, as the stratopause is lowered during SSWs) (Figure 4). This reduction of GW activity is likely due to the existence of GW critical levels caused by the zonal wind weakening or reversal during SSWs, implying GW dissipation and drag on the mean flow at lower altitudes than during undisturbed conditions.

Stratospheric GW amplitudes display large geographic variability. Consistent with some previous studies, GW amplitudes were generally larger at the polar vortex edge, and smaller in the vortex core and outside of the vortex. This association could be due to the possibility that strong polar vortex jet winds allow more transmission of GWs to this altitude range so that they can be discerned in the satellite data.

As the first study to extend the usage of the COSMIC and CHAMP GPS temperature data up to 60 km in altitude, we compare the GPS analysis with independent HIRDLS and

SABER temperature retrievals. We find that the temporal variability of the HIRDLS and SABER zonal mean temperatures generally agrees well with that of the GPS (Figures 1 and 2) up to ~ 60 km. This could have particular implications for polar atmospheric studies because the GPS data have better coverage at very high latitudes (e.g., the COSMIC GPS occultations can routinely reach within 2° of the poles) than other satellite data such as HIRDLS and SABER. The GPS zonal mean temperatures are, however, somewhat less sensitive to warmings than HIRDLS and SABER. GW analysis from GPS is consistent with HIRDLS up to ~ 35 km. At higher altitudes, there is indication that small-scale variability in the GPS data is questionable, though this needs to be investigated further in future studies.

We finally note that there exist different types of SSW events with various characteristics and more observational and modeling studies are needed to gain a more comprehensive and thorough understanding of the relationship between the two phenomena, which has significant implications for improved understanding of both the middle and lower atmosphere.

Acknowledgments.

We appreciate the valuable discussions with Dr. Sergey Sokolovskiy at the University Corporation for Atmospheric Research on the CDAAC GPS RO inversions. We thank Dr. Viktoria Sofieva at the Finnish Meteorological Institute for helpful discussions on this manuscript. We would also like to thank the three anonymous reviewers for their constructive comments. This research was supported by the Climate and Large Scale Dynamics Program of the National Science Foundation grant ATM-0737692. Support for MJA was in part funded by NASA contract NNH06CD16C.

References

Alexander, M. J., 1998: Interpretations of observed climatological patterns in stratospheric gravity wave variance, *J. Geophys. Res.*, **103**, 8627-8640.

Alexander, M. J., and K. H. Rosenlof, 2003: Gravity wave forcing in the stratosphere: Observational constraints from UARS and implications for parameterization in global models, *J. Geophys. Res.*, **108**, D19, 4597, doi:10.1029/2003JD003373.

Alexander, M. J., J. Gille, C. Cavanaugh, M. Coffey, C. Craig, V. Dean, T. Eden, G. Francis, C. Halvorson, J. Hannigan, R. Khosravi, D. Kinneson, H. Lee, S. Massie, B. Nardi, A. Lambert, 2008: Global Estimates of Gravity Wave Momentum Flux from High Resolution Dynamics Limb Sounder (HIRDLS) Observations, *J. Geophys. Res.*, **113**, D15S18, doi:10.1029/2007JD008807.

Alexander, S. P., T. Tsuda, Y. Kawatani, and M. Takahashi, 2008: Global distribution of atmospheric waves in the equatorial upper troposphere and lower stratosphere: COSMIC observations of wave mean flow interactions, *J. Geophys. Res.*, **113**, D24115, doi:10.1029/2008JD010039.

Andrews, D. G., J. R. Holton, and C. B. Leovy, 1987: *Middle Atmospheric Dynamics.* Academic Press, 489 pp.

Baldwin, M. P., and T. J. Dunkerton, 2001: Stratospheric harbingers of anomalous weather regimes. *Science*, **294**, 581-584.

Baumgaertner, A. J. G, and A. J. McDonald, 2007: A gravity wave climatology for Antarctica compiled from Challenging Minisatellite Payload/Global Positioning System (CHAMP/GPS) radio occultations, *J. Geophys. Res.*, **112**, D05103, doi:10.1029/2006JD007504.

de la Torre, A., T. Tsuda, G. A. Hajj, and J. Wickert, 2004: A global distribution of the stratospheric gravity wave activity from GPS occultation profiles with SAC-C and CHAMP, *J. Meteorol. Soc. Jpn.*, **82**(1B), 407-417.

Dowdy, A. J., R. A. Vincent, M. Tsutsumi, K. Igarashi, Y. Murayama, W . Singer, D. J. Murphy, and D. M. Riggin, 2007: polar mesosphere and lower thermosphere dynamics: 2. Response to sudden stratospheric warmings, *J. Geophys. Res.*, **106**, **112**, doi:10.1029/2006JD008127.

Duck, T. J., J. A. Whiteway, and A. I. Carswell, 1998: Lidar observations of gravity wave activity and Arctic stratospheric vortex core warming, *Geophys. Res. Lett.*, **25**, 2813-2816.

Duck, T. J., J. A. Whiteway, and A. I. Carswell , 2001: The gravity wave-arctic stratospheric vortex interaction. *J. Atmos. Sci.*, **58**, 3581-3596.

Dunkerton, T. J., and N. Butchart, 1984: Propagation and selective transmission of internal gravity waves in a sudden warming, *J. Atmos. Sci.*, **41**, 1443-1460.

Garcia, R. R., and B. A. Boville, 1994: “Downward Control” of the mean meridional circulation and temperature distribution of the polar winter stratosphere, *J. Atmos. Sci.*, **51**, 2238-2245.

Gille, J., et al., 2008: The High Resolution Dynamics Limb Sounder (HIRDLS): Experiment overview, results and temperature validation, *J. Geophys. Res.*, doi:10.1029/2007JD008824.

Haynes, P. H., C. J. Marks, M. E. McIntyre, T. G. Shepherd, and K. P. Shine, 1991: On the “downward control” of extratropical diabatic circulations by eddy-induced mean zonal forces, *J. Atmos. Sci.*, **48**, 651-678.

Hei, H., T. Tsuda, and T. Hirooka, 2008: Characteristics of atmospheric gravity wave activity in the polar regions revealed by GPS radio occultation data with CHAMP, *J. Geophy. Res.*, **113**, doi:10.1029/2007JD008938.

Holton, J. R., 1983: The influence of gravity wave breaking on the general circulation of the middle atmosphere. *J. Atmos. Sci.*, **40**, 2497-2507.

Holton, J. R., M. J. Alexander, and M. T. Boehm, 2001: Evidence for short vertical wavelength Kelvin waves in the Department of Energy-Atmospheric Radiation Measurement Nauru99 radiosonde data, *J. Geophys. Res.*, **106**, 20,125-20,129.

Kuo, Y.-H., T.-K. Wee, S. Sokolovskiy, C. Rocken, W. Schreiner, D. Hunt, and R. A. Anthes, 2004: Inversion and error estimation of GPS radio occultation data, *J. Meteorol. Soc. Jpn*, **82**, 507-531.

Lohmann, M.S., 2005: Application of dynamical error estimation for statistical optimization of radio occultation bending angles. *Radio Sci.*, **40**, RS3011, doi:10.1029/2004RS003117.

Marks, C. J., and S. D. Eckermann, 1995: A three-dimensional nonhydrostatic ray-tracing model for gravity waves: Formulation and preliminary results for the middle atmosphere, *J. Atmos. Sci.*, **52**, 1959-1984.

Matsuno, T., 1971: A dynamical model of the stratospheric sudden warmings. *J. Atmos. Sci.*, **28**, 1479-1494.

Matsuno, T., and K. Nakamura, 1979: The Eulerian and Lagrangian-mean meridional circulations in the stratosphere at the time of a sudden warming. *J. Atmos. Sci.*, **36**, 640-654.

Mlynczak, M., and J. Russell, 1995: An overview of the SABER experiment for the TIMED mission, *NASA Langley Research Center, Optical Remote Sensing of the Atmosphere, 2.*

Randel, W., M.-L. Chanin and C. Michaut., 2002: SPARC Intercomparison of Middle Atmosphere Climatologies, *WCRP-116, WMO/TD-No.1142, SPARC Report No.3*, 96 pp.

Ratnam, M. V., T. Tsuda, C. Jacobi, and Y. Aoyama, 2004: Enhancement of gravity wave activity observed during a major Southern Hemisphere stratospheric warming by CHAMP/GPS measurements, *Geophys. Res. Lett.*, **31**, L16101, doi:10.1029/2004GL019789.

Rienecker, M. M., et al., 2008: The GEOS-5 data assimilation system, documentation of versions 5.0.1, 5.1.0, and 5.2.0, *Technical Report series on Global Modeling and Data Assimilation*, NASA/TM-2008-104606, Vol. **27** (http://gmao.gsfc.nasa.gov/pubs/docs/GEOS5_104606-Vol27.pdf).

Rocken, C., Y.-H. Kuo, W. Schreiner, D. Hunt, S. Sokolovskiy, and C. McCormick, 2000: COSMIC system description, *Terr. Atmos. Oceanic Sci.*, **11(1)**, 21-52.

Stockwell, R. G., L. Mansinha, and R. P. Lowe, 1996: Localisation of the complex spectrum: the S-transform, *J. Assoc. Expl. Geophys.*, **XVII**, 99-114.

Trenberth, K. E., 1992: Global Analyses from ECMWF and Atlas of 1000 to 10 mb Circulation Statistics. *TN-373+STR, National Center for Atmospheric Research*, 205 pp.

Tsuda, T., M. Nishida, C. Rocken, and R. H. Ware, 2000: A global morphology of gravity wave activity in the stratosphere revealed by the GPS occultation data (GPS/MET), *J. Geophys. Res.*, **105**, 7257-7273.

Wang, L., D. C. Fritts, B. P. Williams, R. A. Goldberg, F. J. Schmidlin, and U. Blum, 2006: Gravity waves in the middle atmosphere during the MaCWAVE winter campaign: Evidence of mountain wave critical level encounters, *Ann. Geophys.*, **24**, 1209-1226.

Wang, L., M. A. Geller, and M. J. Alexander, 2005: Spatial and temporal variations of gravity wave parameters. Part I: Intrinsic frequency, wavelength, and vertical propagation direction, *J. Atmos. Sci.*, **62**, 125-142.

Ware, R., M. Exnet, D. Feng, M. Gorbunov, K. Hardy, B. Herman, Y. Kuo, T. Meehan, W. Melbourne, C. Rocken, W. Schreiner, S. Sokolovskiy, F. Solheim, X. Zhou, R. Anthes, S. Businger, and K. Trenberth, 1996: GPS sounding of the atmosphere: Preliminary results, *Bull. Am. Meteorol. Soc.*, **77**, 19-40.

Yunck, T. P., G. F. Lindal, and C. H. Liu, 1988: The role of GPS in precise earth observation, paper presented at the *IEEE Position, Location and Navigation Symposium*, Inst. of Electr. and Electron. Eng., Orlando, Fla., 29 Nov. to 2 Dec.

Zhang, F., S. E. Koch, C. A. Davis, and M. L. Kaplan, 2001: Wavelet analysis and the governing dynamics of a large-amplitude gravity wave event along the East Coast of the United States, Q. J. R. Meteorol. Soc., **127**, 2209-2245.

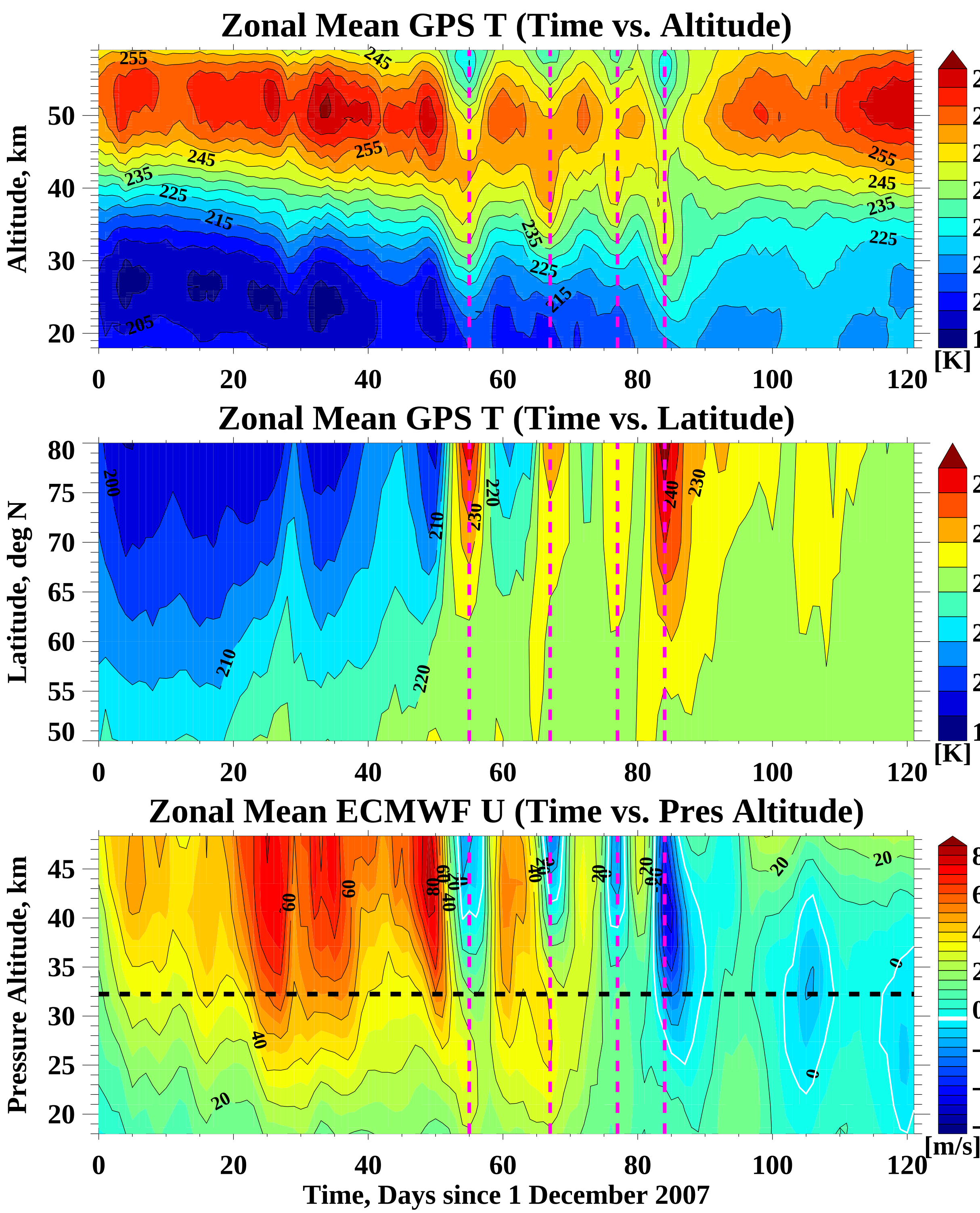

Figure 1: Top: time-altitude contour of zonal mean GPS temperature at 70°N; Middle: time-latitude contour of zonal mean GPS temperature at 30 km; Bottom: time-pressure altitude contour of zonal mean zonal wind at 65°N from the ECMWF reanalysis. The red dashed lines mark the warming events identified. The black dashed line on the bottom panel marks the 10 hPa level.

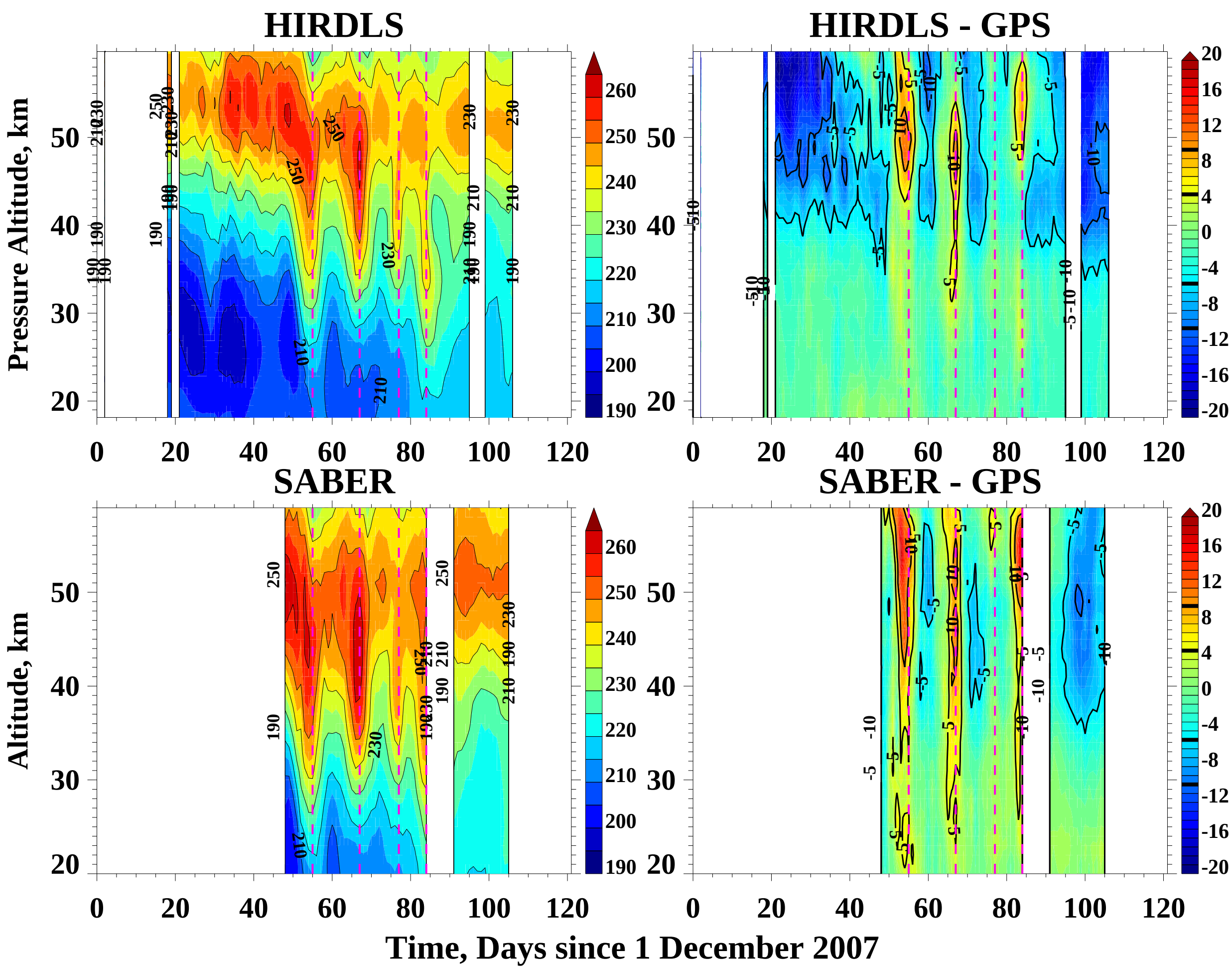

Figure 2: Top left: time-pressure altitude contour of zonal mean temperatures from HIRDLS; Bottom left: time-altitude contour of SABER temperatures; Right column: temperature differences between HIRDLS/SABER and GPS.

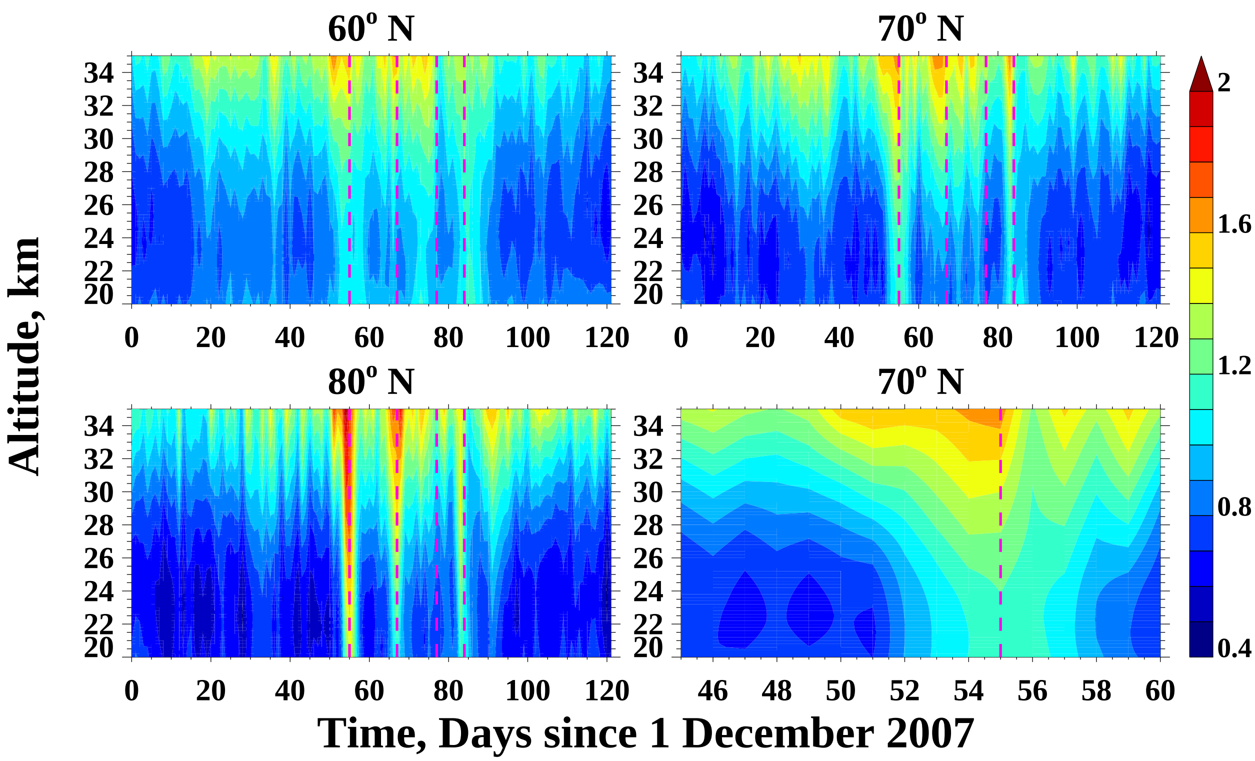

Figure 3: Time-altitude contours of gravity wave amplitudes at 60, 70, and 80°N from GPS temperature retrievals. The lower-right panel shows the blowup contour image around the first minor warming event at 70°N.

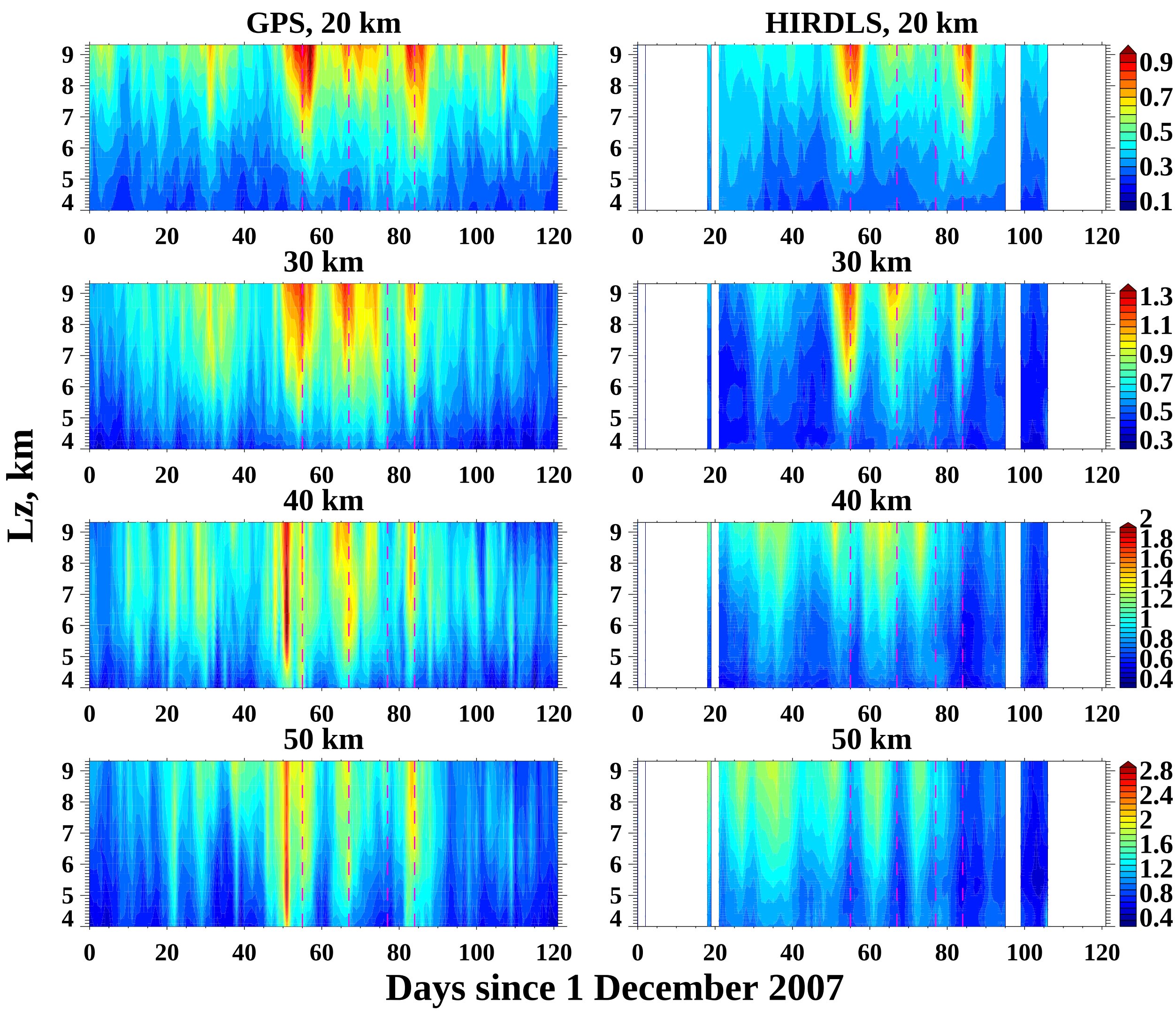

Figure 4: Time-vertical wavelength contour of zonal mean gravity wave amplitude at 70° from GPS (left column) and HIRDLS (right column) at selected altitudes.

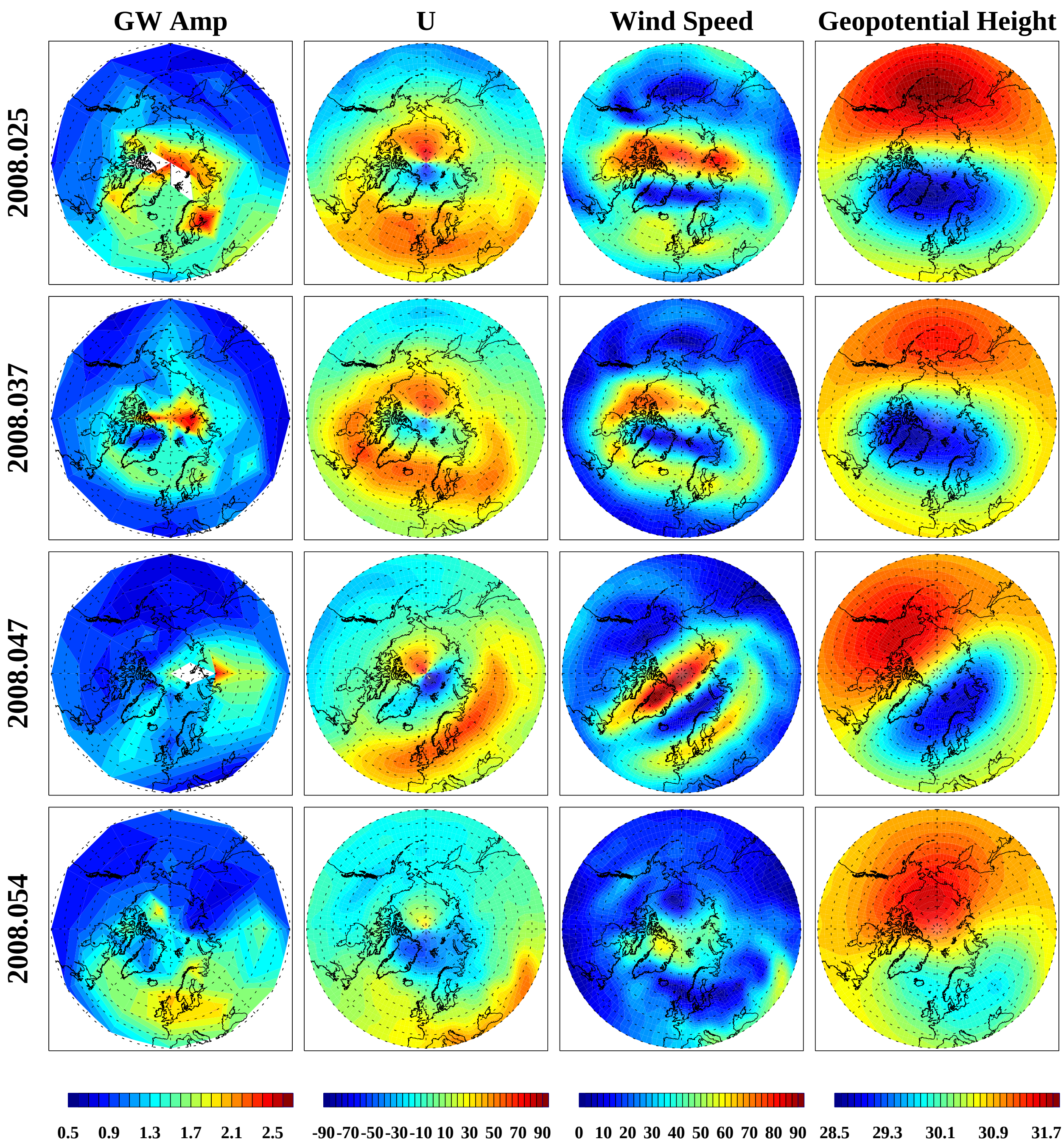

Figure 5: Stereographic projected daily mapped contour of gravity wave amplitude averaged between 30 and 35 km (left-most column) from GPS, and zonal velocity component (second column), wind speed (third column), and geopotential height (right-most cloumn) at 10 hPa from the ECMWF reanalysis. The four rows are for 25 January, 2 February, 16 February, and 23 February of 2008 (i.e., the four warming events identified in Figure 1), respectively.

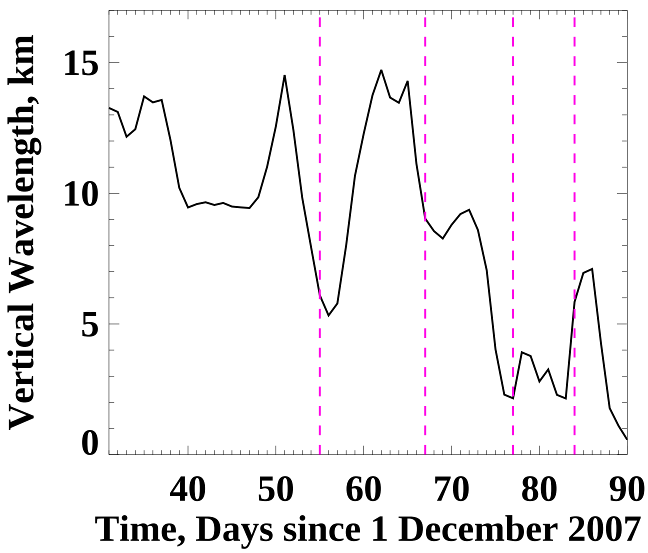

Figure 6: Vertical wavelength of a zonally propagating stationary gravity wave derived from Equation (1). See text for more details.

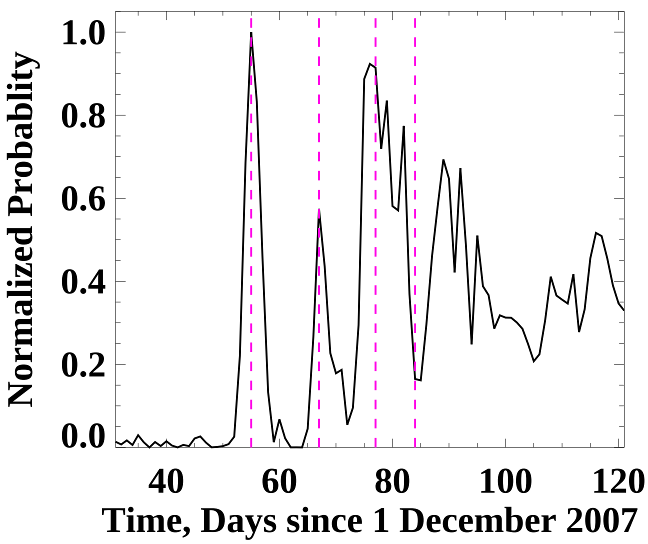

Figure 7: Normalized probability of observing a GW with vertical wavelength between 4 and 10 km in the altitude range of 25 to 35 km from ray-tracing simulations using background winds and temperatures at 70°N derived from the GEOS-5 analysis data. A constant source spectrum with phase speed between -10 and 10 ms^{-1} and horizontal wavelength of 100 km is used. The rays are launched at an altitude of 10 km. See text for more details.